The Inductance Enhancement Study of Spiral Inductor Using Ni–AAO Nanocomposite Core

M. C. Hsu, T. Y. Chao, Y. T. Cheng, C. M. Liu, and C. Chen

***Abstract*—The letter presents the fabrication and characterization of on-chip spiral inductors with Ni–anodic alumina oxide (Ni–AAO) nanocomposite core. Ni nanorods with 70 nm diameter are deposited and isolated in an AAO matrix to form a layer of nanocomposite on silicon substrate. About 3% inductance enhancement to the inductor with the nanocomposite core has been observed and the enhancement can be kept up more than 6 GHz. Because the proposed inductance enhancement scheme using ferromagnetic–AAO-based nanocomposite as inductor core employs a CMOS-compatible fabrication process with the characteristics that can be further improved, it is our belief that the scheme has a great potential application for future radio frequency integrated circuitry (RFIC) manufacture.**

***Index Terms*—Anodic alumina oxide (AAO), inductance, magnetic resonance, Ni–anodic alumina oxide (Ni–AAO) nanocomposite core, Ni nanorods, quality (Q) factor, spiral inductor.**

I. Introduction

HOW TO practically employ ferromagnetic material as a core to increase the inductance of on-chip spiral inductor is always an important research topic in the development of radio frequency integrated circuitry (RFIC) technology. An inductance enhancement scheme can not only reduce chip area occupied by the inductors for low manufacturing cost but also strengthen Q performance of the inductors for high-performance RFIC applications [1]. The Q performance is associated with the signal transmission loss in an on-chip inductor, including the induced eddy current loss originated from the substrate underneath itself and the resistive loss coming from the structure material, aluminum or copper. In general, loss reduction can be realized using micromachined technique to fabricate a cavity under the coil to reduce the eddy current loss and utilizing connected metal lines by metal via to increase coil conductance [2], [3]. Since the size of inductor can be shrunk via the incorporation of ferromagnetic material, higher Q performance of inductor can be further driven with less eddy current and resistive losses.

Manuscript received August 21, 2008; revised February 4, 2009. First published February 27, 2009; current version published May 6, 2009. This work was supported in part by the National Security Council (NSC) of R.O.C. under Grant NSC 96-2220-E-009-024 and in part by the System-on-a-Chip (SoC) Technology Center (STC), Industrial Technology Research Institute (ITRI). The review of this paper was arranged by Associate Editor D. Litvinov.

M. C. Hsu, T. Y. Chao, and Y. T. Cheng are with the Microsystems Integration Laboratory, Department of Electronics Engineering, National Chiao Tung University (NCTU), Hsinchu 300, Taiwan (e-mail: mchsu.ee95g@nctu.edu.tw; buck34.ee92g@nctu.edu.tw; ytcheng@mail.nctu.edu.tw).

C. M. Liu and C. Chen are with the Department of Materials Science and Engineering, National Chiao Tung University (NCTU), Hsinchu 300, Taiwan (e-mail: amin6397@yahoo.com.tw; chih@faculty.nctu.edu.tw).

Color versions of one or more of the figures in this paper are available online at http://ieeexplore.ieee.org.

Digital Object Identifier 10.1109/TNANO.2009.2015758

Nevertheless, there is still a technical challenge in the development of the inductor with ferromagnetic core. The inductor usually accompanies with poor performance at high frequency due to FMR effect and the eddy current loss occurrence in the layer of magnetic material [4]. According to the simplified Landau–Lifshitz–Gilbert equation [5], the FMR frequency of ferromagnetic film can be calculated as follows:

$$f_{\mathrm{FMR}} \cong \frac{\gamma}{2\pi}\sqrt{H_k\left(H_k + 4\pi M_s\right)} \tag{1}$$

where γ, H_k, and M_s are gyromagnetic ratio, i.e., 176 GHz/T, anisotropy magnetic field, and saturated magnetization, respectively. The frequency usually falls in a range of several hundred megahertz to 1 GHz, which is coincident with the operational frequency range of the present wireless carrier frequencies. Since FMR effect would result in large inductance variance in the region nearby the resonant frequency, such an inductor with ferromagnetic core is not suitable for RFIC applications.

According to (1), the increase of both H_k and M_s can effectively inhibit the occurrence of FMR effect by shifting the resonant frequency to several gigahertz range. Recently, Yamaguchi *et al.* have proposed patterned magnetic CoNbZr layer [6] to modify demagnetizing field distribution for having H_k enhancement that can result in a higher FMR frequency up to 2 GHz. Viala *et al.* have demonstrated 100% hard axis excitation to ensure high H_k performance simply by devising $\mathrm{FeH_fN}$ laminated film only under the metal structure of inductor [7]. Jiang *et al.* further proposed and employed anitferromagnetic/ferromagnetic multilayers (IrMn/CoFe) to increase H_k via the exchange-coupled mechanism without having any Q performance degradation [8]. Although these approaches can achieve the inductance enhancement and eliminate the disturbance resulted by FMR phenomenon, CMOS-incompatible material, and complex fabrication processes make themselves not fascinating for real CMOS on-chip spiral inductor fabrication. Besides, it is still inevitable to have the eddy current loss existing in the layer of the magnetic materials.

Ni has been widely used for CMOS backend under bump metallization (UBM) process and is also a stable ferromagnetic material. Recent investigations have shown that the rod-like shape and nanometer size of magnetic material could have higher anisotropy magnetic field H_k [9]. Meanwhile, Liu and Chen, have successfully synthesized Ni nanorods using electroless deposition and demonstrated superparamagnetic characteristics [10]. Since the Ni nanorods is grown within anodic alumina oxide (AAO) template, which is an electrical insulator and can isolate each nanorod to effectively reduce the eddy current loss in the layer of the magnetic materials, a fully CMOS-compatible process is proposed and developed in this paper for

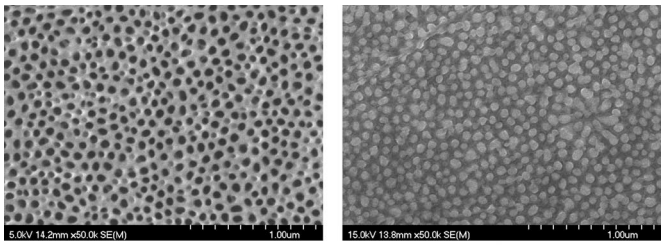

Fig. 1. SEM photographs of the top views of (a) AAO template and (b) Ni nanorods (AAO removed).

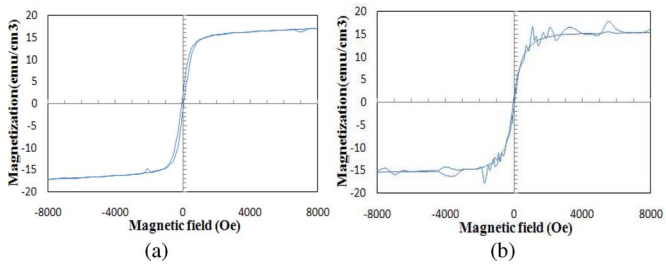

Fig. 2. M–H loops of Ni–AAO nanocomposite with different forms of applied magnetic fields. (a) Out-of-plane. (b) In-plane.

high-performance spiral inductor fabrication in which Ni–AAO nanocomposite layer is incorporated as magnetic core. The related material synthesis, characterization, and device fabrication and performance measurement are depicted in detail as follows.

II. Nanocomposite Synthesis and Inductor Fabrication

A. Ni–AAO Nanocomposite Synthesis and Characterization

Porous AAO with uniformly self-organized hexagonal nanopores is made as the template for 1-D Ni nanorod synthesis. The template can be fabricated by anodizing Al film in various acidic solutions with certain processing parameters, such as applied voltage, current, temperature, and time, which are strongly correlated with the diameter and length of the pore [11], [12]. In this study, AAO template is first synthesized by one-step anodizing process where Al film is applied with 40 V in a 0.3 M oxalic acid ($H_2C_2O_4$) solution at room temperature until the film is fully oxidized. The oxidized film is then annealed at 400 °C for 2 h for structure strengthening. After the thermal anneal, the AAO template is put in a 5% H_3PO_4 solution at 30 °C for 50 min to form a uniformly distributed nanopore structure with the size of 70 nm in diameter, as shown in Fig. 1(a).

For the synthesis of Ni–AAO nanocomposite, the as-fabricated AAO template is first dipped into $SnCl_2$ and $PdCl_2$ solutions for 2 min and 30 s, respectively, for AAO surface activation, which is followed by electroless Ni deposition at 60 °C for 1 min. Once the top surface of Ni–AAO nanocomposite film is mechanically polished to remove overplated Ni layer, the composite with electrically isolated Ni nanorods, as shown in Fig. 1(b), is rapid thermally annealed (RTA) at 400 °C for 2 min for better magnetic characteristics [10], which can then be used for following inductor fabrication.

According to the previous investigations, the easy axis and hard axis of ferromagnetic nanorods/nanowires [13], [14] would be along out-of-plane and in-plane directions, respectively, due to a large aspect ratio of rod/wire length to diameter. Fig. 2 shows the superconducting quantum interference device (SQUID) measurements of Ni–AAO nanocomposite, which are applied with in-plane and out-of-plane magnetic fields, respectively. The relative permeability of the nanocomposite can be calculated from the slope of M–H curve as follows:

$$\mu_r = 1 + \frac{4\pi M}{H_0} \tag{2}$$

where H_0 and M are applied magnetic field and corresponding magnetization in Gaussian unit, respectively. The relative permeabilities of the composite at 10 Oe are 1.8 and 1.75 for the out-of-plane and in-plane applied fields, respectively. The measurement results also indicate that the Ni–AAO nanocomposite has little anisotropic behavior, which is very similar to the nanowire behavior [13]. In addition, from (1), the FMR frequency of ferromagnetic film is estimated about as high as 5.3 GHz due to large H_k, which is about 1700 Oe.

B. Inductor Fabrication

In this study, the spiral inductors of 3.5 and 4.5 turns, which are made of 5-μm-thick electroplated Cu and designed with 100 μm in inner diameter, 15 μm in line width, and 5 μm in line spacing, are utilized for characterizing the inductance enhancement using the Ni–AAO nanocomposite core. Fig. 3 illustrates the process flow of the spiral inductor fabrication. It begins with 0.7-μm-thick thermal oxidization on a p-type (1 0 0) silicon substrate. Then, a 1-μm-thick Al film is deposited for AAO template fabrication, as shown in Fig. 3(a). Then, the Ni–AAO nanocomposite film is fabricated using the aforementioned one-step anodic-oxidation method followed by electroless Ni plating, as shown in Fig. 3(b) and (c), respectively. Same RTA process is performed at 400 °C for 2 min for Ni crystallization. As Fig. 3(d) shows, a layer of 0.2-μm-thick SiO_2 is then sputtered on the top of the composite film as an electrical insulation layer followed by Cr/Cu (300Å/900Å) adhesion/seed layer deposition for following Cu plating process for spiral inductor fabrication.

For the inductor fabrication, a 6-μm-thick AZ4620 photoresist (PR) layer is first spun and photo-patterned as the plating mold for the coil fabrication of the spiral inductor, as shown in Fig. 3(e). After 5-μm-thick Cu electroplating, a 10-μm-thick AZ4620 PR is spun, patterned, and sputtered with another 150 nm Cu seed layer for the via filling of Cu air bridge, which is followed by another 10-μm-thick AZ4620 PR spin coating. As Fig. 3(f) shows, the coated AZ4620 PR is then patterned as the mold for air bridge beam fabrication. Once a 5-μm-thick Cu is electroplated to form the air bridge, the fabrication of the spiral inductor is then finished right after removing the underneath Cu seed layer, which is chemically etched away using Cu and Cr etchants [15]. Fig. 4 shows an as-fabricated 3.5-turn spiral inductor with magnetic Ni–AAO nanocomposite core.

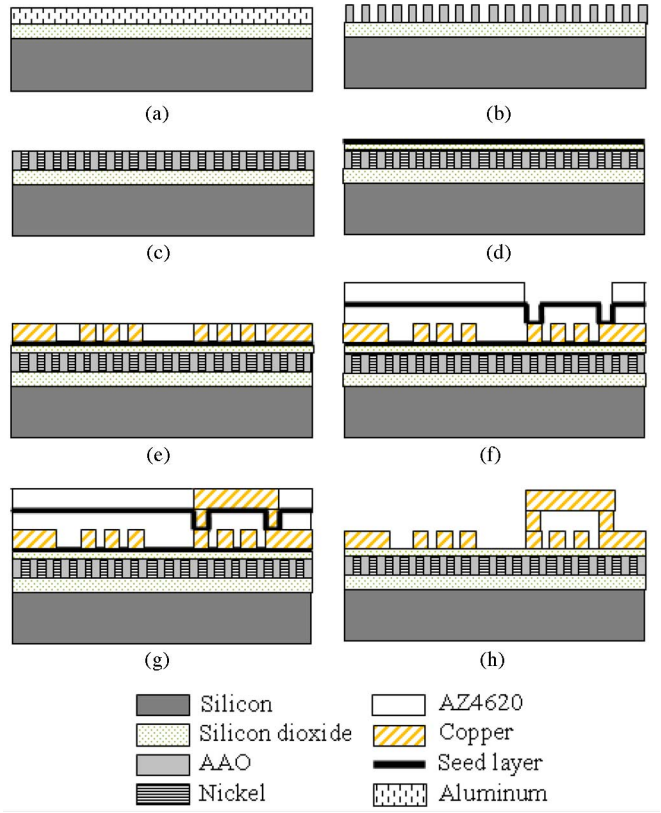

Fig. 3. Fabrication process flow. (a) SiO_2 and Al layer deposition. (b) Al anodized as AAO template. (c) Electroless Ni plating. (d) SiO_2 and Cr/Cu seed/adhesion layer deposition. (e) First Cu plating for the coil part of the inductor. (f) Air bridge seed layer deposition and patterning. (g) Air bridge and via plating. (h) Seed layer and PR removal.

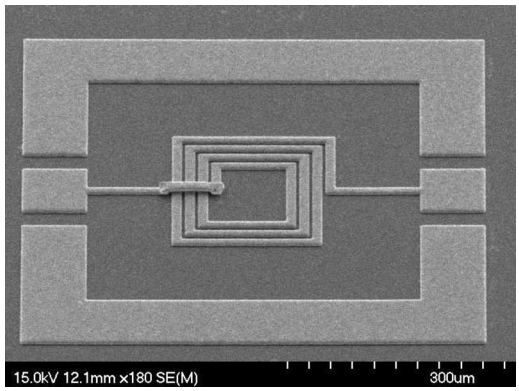

Fig. 4. SEM photograph of as-fabricated on chip spiral inductors with Ni–AAO nanocomposite.

III. Measurement and Discussion

In the experiment, the two-port scattering parameters (S-parameters) of the inductors are measured up to 20 GHz with an on-wafer probe station using the high-frequency probes (Cascade Microtech, Inc., ACP-40-GSG-100 μm) and Agilent E8364B PNA network analyzer. The parasitic parallel capacitance between the contact pads of inductor is de-embedded using the measured result of designed dummy pattern [16]. The de-embedded S-parameters are then transformed into Y-parameter,

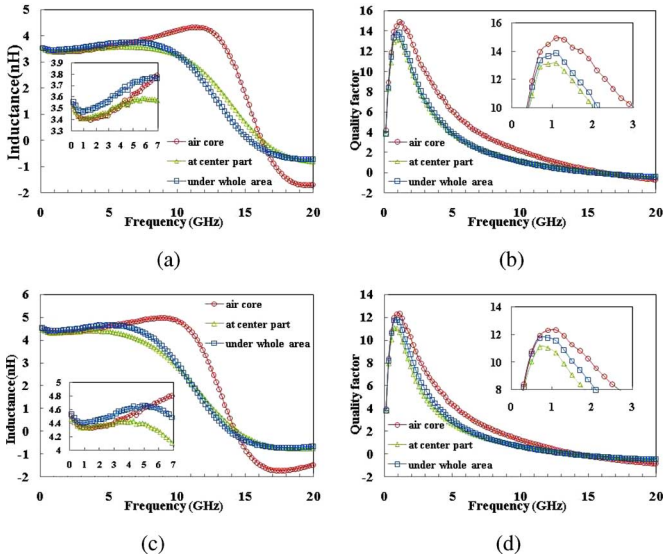

Fig. 5. Measured high-frequency characteristics of spiral inductors with Ni–AAO nanocomposite core. (a) Inductance of spiral inductor with $N = 3.5, d_{\text{in}} = 100\,\mu$m. (b) Q-factor of spiral inductor with $N = 3.5, d_{\text{in}} = 100\,\mu$m. (c) Inductance of the spiral inductor with $N = 4.5, d_{\text{in}} = 70\,\mu$m. (d) Q-factor of the spiral inductor with $N = 4.5, d_{\text{in}} = 70\,\mu$m.

and the equivalent series inductance (L) and quality factor (Q) of inductor are extracted from the Y-parameters based on the following equation [15], [16], respectively:

$$L = \frac{\text{Im}(1/Y_{11})}{2\pi f} \tag{3}$$

$$Q = \frac{\text{Im}(1/Y_{11})}{\text{Re}(1/Y_{11})} \tag{4}$$

where f is the signal frequency. The frequency-dependent inductance and Q-factor of the fabricated inductors are depicted in Fig. 5. Fig. 5(a) and (b) shows that the spiral inductor of 3.5 turns with Ni–AAO nanocomposite magnetic core can have 3% larger inductance (3.58 nH at 3 GHz) than that of inductor without the core (3.47 nH at 3 GHz), and the enhancement trend has been kept up to 6.9 GHz. Meanwhile, the maximum Q-factor decreases from 15 to 14 at 1.1 GHz, which is about 6.7% reduction. Similar inductance enhancement and Q degradation also occur in the case of the spiral inductor of 4.5 turns. The spiral inductor of 4.5 turns with Ni–AAO nanocomposite magnetic core can have about 2.5% larger inductance (4.54 nH at 3 GHz) than that of inductor without the core (4.43 nH at 3 GHz) but the Q decreases from 12 to 11.6 at 1.1 GHz, which is also about 6.5% reduction.

In general, the magnetization of a ferromagnetic material along easy axis (out-of-plane in this case) and hard axis (in-plane in this case) are dominant by domain wall motion and spin rotation, respectively. Thus, the relative permeability along easy axis is larger than that along hard axis and the hard axis excitation would determine the FMR characteristics of the material while the material is applied with a time-variant magnetic field at higher frequency. In the Ni–AAO nanocomposite system, SQUID measurement has shown little anisotropic behavior that further indicates that the magnetization along both axes

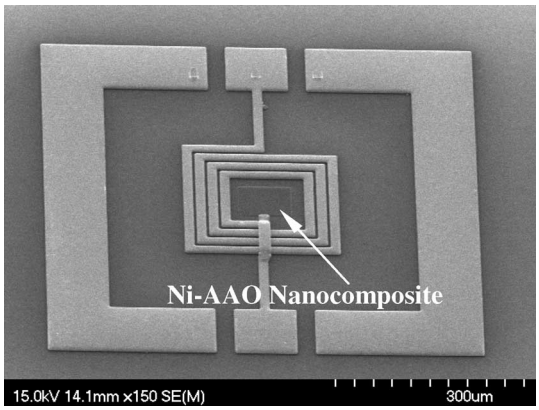

Fig. 6. SEM photograph of as-fabricated on-chip spiral inductor with the Ni–AAO nanocomposite only in the central region.

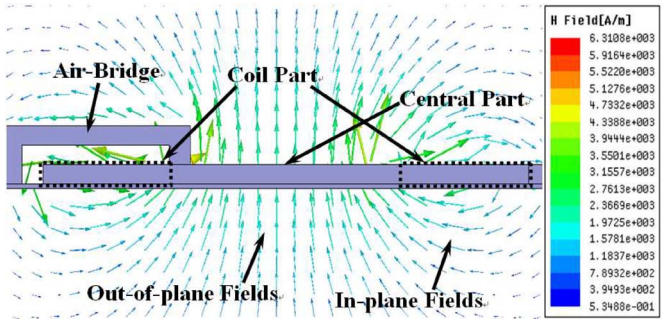

Fig. 7. Simulated magnetic field distribution of spiral inductor using Ansoft HFSS.

would contribute the inductance enhancement of spiral inductor. In order to verify the hypothesis, the spiral inductor with the Ni–AAO nanocomposite core only placed in the central part of spiral inductor is fabricated as shown in Fig. 6.

For both cases of the spiral inductors of 3.5 and 4.5 turns, no noticeable inductance enhancement of the inductor has been found in the high-frequency measurement. On the other hand, the measurement shows that the maximum Q-factors of the inductors decrease from 15 to 13.2 at 1.1 GHz, and 12 to 10.7 at 1.1 GHz, respectively. More than 12% Q reduction has been found in the inductors using the Ni–AAO nanocomposite core only placed inside the spiral inductor. The worse Q performance can be attributed to little inductance enhancement. For a conventional on-chip spiral inductor, the Q can be depicted as the following equation [17]:

$$Q = \frac{\omega L_s}{R_s} \cdot \frac{R_p}{R_p + [(\omega L_s/R_s)^2 + 1]R_s} \times \left[1 - \frac{R_s^2(C_s + C_p)}{L_s} - \omega^2 L_s(C_s + C_p)\right] \quad (5)$$

where L_s, R_s, C_s, C_p, R_p, and ω are the inductance, series resistance, and series feed-forward capacitance of the inductor, parasitic shunt capacitance, resistance, and signal frequency, respectively. In addition to the first term in (5), Q is, in fact, associated with energy loss terms that are the rest terms of (5) all with the values less than 1. When a magnetic core is implemented to a spiral inductor, an additional term associated with magnetic loss will be introduced into the equation and result in the Q-factor reduction. Therefore, the total Q-factor would decrease as expected once the inductance enhancement of the spiral inductor with Ni–AAO nanocomposite core in the center is minute.

Fig. 7 shows the simulated magnetic field distribution in a spiral inductor with a 3 GHz electromagnetic wave signal input using Ansoft HFSS. The distribution indicates the magnetic field in the central part of inductor and the part underneath the coil structure would mainly be out-of-plane and in-plane fields, respectively. Since both types of magnetizations have very similar M–H characteristics, the magnetizations would simultaneously contribute to the total inductance enhancement. In comparison with the total area of Ni–AAO nanocomposite core that fully covers the whole area of spiral inductor and provides only 3% inductance enhancement, the area of Ni–AAO nanocomposite only placed in the central region of the inductor is about one-tenth of the total area or even smaller. Therefore, it can be expected with minute inductance enhancement and worse Q performance when the Ni–AAO nanocomposite is only implemented in the central region of spiral inductor.

Although there is only 3% inductance enhancement in the work, the magnetic properties can be further enhanced by improving the permeability of the composite material, such as increasing the porosity of AAO for more Ni incorporation in the composite, thermally annealing the electroless deposited Ni for the phosphorus content reduction [18], and using electroless CoP, CoNiP, or NiFe that has larger permeability instead of Ni [19] for nanocomposite synthesis, etc. On the other hand, further investigation is required regarding the Q degradation. As aforementioned, Q-factor is a tradeoff of inductance enhancement and magnetic loss. In fact, the propagation loss of EM signal in Ni–AAO nanocomposite should be also considered. As long as the detail loss mechanism can be well understood, it can be expected that the size of inductor can be effectively shrunk via the incorporation of ferromagnetic material for higher Q performance of inductor due to less eddy current and resistive losses.

IV. Conclusion

The high-frequency characteristics of on-chip spiral inductor with Ni–AAO nanocomposite core have been investigated. Incorporated with the nanocomposite core, the 3.5- and 4.5-turn inductors can have improved inductance up to 6.9 and 5.5 GHz, respectively, without having any observable FMR phenomenon. Although insignificant inductance enhancement and Q degradation have been found in the inductors with the nanocomposite core, it could be further improved such as the porosity increase of AAO, phosphorus content reduction of Ni, and the incorporation of ferromagnetic metal with larger permeability. Because the size of inductor can be shrunk via the incorporation of ferromagnetic material based on a CMOS-compatible fabrication scheme, high-performance inductor can be expected with less eddy current and resistive losses.

ACKNOWLEDGMENT

Authors would like to thank National Center of High-Performance Computing (NCHC) for the simulator support and for the support of EM simulator and the Instrument Center at National Chiao Tung University (NCTU) for the support of fabrication facility and SQUID measurement.

REFERENCES

[1] C. Y. Yue and S. S. Wong, "On-chip spiral inductors with patterned ground shields for Si-based RF IC's," *IEEE J. Solid-State Circuits*, vol. 33, no. 5, pp. 743–753, May 1998.

[2] J. W. Lin, C. C. Chen, and Y. T. Cheng, "A robust high-Q micromachined RF inductor for RFIC applications," *IEEE Trans. Electron Devices*, vol. 52, no. 7, pp. 1489–1496, Jul. 2005.

[3] J. Kim, J.-O. Plouchart, N. Zamdmer, N. Fong, L.-H. Lu, Y. Tan, K. A. Jenkins, M. Shcrony, R. Groves, M. Kumar, and A. Ray, "High-performance three-dimensional on-chip inductors in SOI CMOS technology for monolithic RF circuit applications," in *Proc. IEEE MTT-S Int. Microw. Symp. Dig.*, 2003, pp. 77–80.

[4] V. Korenivski, "GHz magnetic film inductors," *J. IMMM.*, vol. 215, pp. 800–806, 2000.

[5] R. C. O'Handley, *Modern Magnetic Materials*. New York: Wisley Interscience, 2000.

[6] M. Yamaguchi, M. Ba ba, and K. I. Arai, "Sandwich-type ferromagnetic RF integrated inductor," *IEEE Microw. Theory Tech.*, vol. 36, no. 7, pp. 620–628, Jul. 2005.

[7] B. Viala, S. Couderc, A. S. Royet, P. Ancey, and G. Bouche, "Bidirectional ferromagnetic spiral inductors using single deposition," *IEEE Trans. Magn.*, vol. 41, no. 10, pp. 3544–3549, Oct. 2005.

[8] R. F. Jiang, N. N. Shams, M. T. Rahman, and C. H. Lai, "Exchange-coupled IrMn/CoFe mulitlayers for RF-integrated inductors," *IEEE Trans. Magn.*, vol. 43, no. 10, pp. 3930–3932, Oct. 2007.

[9] N. Cordente, M. Respaud, F. Senocq, M. Casanove, C. Amiens, and B. Chaudret, "Synthesis and magnetic properties of nickel nanorods," *Nano Lett.*, vol. 1, pp. 565–568, 2001.

[10] C. M. Liu and C. Chen, "Microstructure and magnetic properties of nickel nanorod arrays on silicon substrate," *TMS Conf., TMS,* Orlando, FL, 2007.

[11] S. Shingubara, "Fabrication of nanomaterials using porous alumina templates," *J. Nanopart. Res.*, vol. 5, pp. 17–30, 2003.

[12] M. M. Sinha and J. S. Kim, "Analysis of vibrational modes and phonon density of statesof aluminate spinels," *J. Korean Phys. Soc.*, vol. 43, no. 2, pp. 237–241, Aug. 2003.

[13] J.-S. Jung, L. Malkinski, J.-H. Lim, M. Yu, C. J. O'Connor, H.-O. Lee, and E.-M. Kim, "Fabrication and magnetic properties of Co nanostructures in AAO membranes," *Bulletin Korean Chem. Soc.*, vol. 29, no. 4, pp. 758–760, Apr. 2008.

[14] C. A. Ramos, E. V. Brigneti, D. Navas, K. Pirota, and M. Vazquez, "Variable-size Ni magnetic nanowires as observed by magnetization and ferromagnetic resonance," *Phys. B: Condens. Matter*, vol. 384, no. 1–2, pp. 19–21, Oct. 2006.

[15] J.-W. Lin, C. C. Chen, and Y.-T. Cheng, "A robust high-Q micromachined RF inductor for RFIC applications," *IEEE Trans. Electron Devices*, vol. 52, no. 7, pp. 1489–1496, Jul. 2005.

[16] I. J. Bahl, "High-performance inductors," *IEEE Trans. Microw. Theory Tech.*, vol. 49, no. 4, pp. 654–664, Apr. 2001.

[17] C. Y. Yue and S. S. Wong, "On-chip spiral inductors with patterned ground shields for Si-based RFIC's," in *Proc. IEEE, JSSC*, May 1998, vol. 33, no. 5, pp. 743–753.

[18] B. Szpunar, M. Aus, C. Cheung, U. Erb, G. Palumbo, and J. A. Szpunar, "Magnetism in nanostructured Ni–P and Co-W alloys," *J. Magn. Magn. Mater.*, vol. 187, no. 3, pp. 325–336, Sep. 1998.

[19] N. V. Myung, P. T. A. Sumodjo, D.-Y. Park, and B.-Y. Yoo, "Development of electroplated magnetic materials for MEMS," *J. Magn. Magn. Mater.*, vol. 265, no. 2, pp. 189–198, Sep. 2003.

Author's photographs and biographies not available at the time of publication.